Electronic Supporting Information

The Homometallic Polyoxotungstate Archetype {P_4W_{24}}

Xiaofeng Yi,[a,b] Natalya V. Izarova,[a] and Paul Kögerler [a,b,*]

a. Jülich-Aachen Research Alliance (JARA-FIT) and Peter Grünberg Institute (PGI 6), Forschungszentrum Jülich, D-52425 Jülich, Germany.
b. Institute of Inorganic Chemistry, RWTH Aachen University, D-52074 Aachen, Germany.

I. General methods and materials.

The reagents were used as purchased without further purification. $K_{12}[H_2P_2W_{12}O_{48}]\cdot 24H_2O$ (**K-P_2W_{12}**) was synthesized according to the reported procedure [1] and its identity and purity were confirmed by IR spectroscopy. Elemental analysis results (ICP-OES and C/H/N) were obtained from Central Institute for Engineering, Electronics and Analytics (ZEA-3), Forschungszentrum Jülich GmbH (D-52425 Jülich, Germany). TGA/DTA measurements were carried out with a Mettler Toledo TGA/SDTA 851 in dry N_2 (60 mL min^{-1}) at a heating rate of 5 K min^{-1}. Vibrational spectra were recorded on a Bruker VERTEX 70 FT-IR spectrometer coupled with a RAM II FT-Raman module (1064 nm Nd:YAG laser) on KBr disks for the FT-IR and the solid material for the Diamond ATR FT-IR and Raman measurements. ^{31}P NMR spectra were recorded by Central Institute for Engineering, Electronics and Analytics (ZEA-3), Forschungszentrum Jülich GmbH (D-52425 Jülich, Germany). The measurements were done at room temperature in 5 mm tubes using a Bruker Avance 600-MHz spectrometer equipped with a prodigy probe, operating at 242.95 MHz for ^{31}P and with a Varian Inova 400 MHz spectrometer equipped with an Auto-X-PFG-probe and with resonance frequency of 161.834 MHz. Chemical shifts are reported with respect to 85% H_3PO_4; all chemical shifts downfield of the reference are reported as positive values. UV-Vis spectra were measured using 10 mm quartz cuvettes on Shimadzu UV-3600 plus UV-Vis-NIR spectrophotometer and Analytik Jena Specord S600 spectrophotometer.

Synthesis of $K_{3.5}Li_8[(CH_3)_2NH_2]_{4.5}[(C_6H_5PO)_2P_4W_{24}O_{92}]\cdot 35H_2O$ (KLD-1).

A solution of $C_6H_5PO_3H_2$ (0.040 g, 0.25 mmol) in 5 mL of 1 M LiCl was added dropwise to a solution of **K-P_2W_{12}** (0.394 g, 0.1 mmol) in 15 mL of 1 M LiCl acidified by 50 μL glacial acetic acid under vigorous stirring. The pH of the resulting mixture was adjusted to 2.5 – 3.0 by addition of glacial acetic acid. The reaction solution was then placed in an oven and uniformly heated at 60 °C for 1 day. After cooling down to room temperature, 1 M aqueous solution of $[(CH_3)_2NH_2]Cl$ (40 drops) was added to the reaction mixture and it was left for evaporation. Transparent colorless block-like crystals of **KLD-1** formed within three weeks. The crystals were collected by filtration and dried in air. Yield: 0.064 g (17.6 % based on $\{P_2W_{12}\}$). Elemental analysis: calculated for $C_{21}H_{116}K_{3.5}Li_8N_{4.5}O_{129}P_6W_{24}$ (found): C, 3.46 (3.47); H, 1.60 (1.60); K, 1.88 (1.90); Li, 0.76 (0.78); N, 0.87 (0.84); P, 2.55 (2.54); W, 60.55 (58.3) %. IR spectrum (KBr pellet), cm^{-1}: 3432 (s, br); 1631 (m); 1466 (w); 1438 (w); 1161 (m); 1128 (m); 1088 (m); 1020 (m); 989 (m); 974 (m); 929 (s); 916 (s); 808 (s); 698 (s); 563 (m); 548 (m); 465 (m). Raman (solid sample, λ_e = 1064 nm), cm^{-1}: 1001(w); 964 (s); 862 (w); 660 (w); 397 (w); 228 (m); 193 (m); 77 (m). UV-Vis (1 M LiCl solution): λ = 213 nm, $\varepsilon = 2.87\times10^5$ $M^{-1}cm^{-1}$; λ = 271 nm, $\varepsilon = 9.49\times10^4$ $M^{-1}cm^{-1}$.

Synthesis of $K_{3.5}Li_8[(CH_3)_2NH_2]_{4.5}[(C_6H_5AsO)_2P_4W_{24}O_{92}]\cdot 40H_2O$ (KLD-2).

The synthetic procedure for **KLD-2** was similar to that for preparation of **KLD-1** but $C_6H_5AsO_3H_2$ (0.051 g, 0.25 mmol) was used instead of $C_6H_5PO_3H_2$. After the reaction 30 drops of 1 M aqueous $[(CH_3)_2NH_2]Cl$ solution were added to the reaction mixture for crystallization. Transparent block-like crystals of **KLD-2** were obtained within four weeks. The crystals were collected by filtration and dried in air. Yield: 0.116 g (31 % based on $\{P_2W_{12}\}$). Elemental analysis: calculated for $C_{21}H_{126}As_2K_{3.5}Li_8N_{4.5}O_{134}P_4W_{24}$ (found): C, 3.38 (3.32); H, 1.70 (1.73); As, 2.01 (2.00); K, 1.83 (1.83); Li, 0.74 (0.72); N, 0.84 (0.81); P, 1.66 (1.62); W, 59.11 (58.6) %. IR spectrum (KBr pellet), cm^{-1}: 3426 (s, br); 1629 (m); 1466 (w); 1440 (w); 1161 (m); 1086 (m); 1018 (m); 989 (m); 929 (s); 916 (s); 829 (s); 785 (s); 694 (s); 573 (m); 528 (m); 465 (m). Raman (solid sample, λ_e = 1064 nm), cm^{-1}: 1001(w); 960 (s); 892 (w); 835 (w); 684 (w); 233 (m); 193 (m); 137 (m); 75 (m). UV-Vis (1 M LiCl solution): λ = 209 nm, $\varepsilon = 2.81\times10^5$ $M^{-1}cm^{-1}$; λ = 270 nm, $\varepsilon = 8.86\times10^4$ $M^{-1}cm^{-1}$.

Synthesis of $H_2K_2Li_{1.5}[(CH_3)_2NH_2]_{4.5}\{[Co(H_2O)_4]_2[\{(H_2O)_4Co\}(C_6H_5PO)_2P_4W_{24}O_{92}]\}\cdot 28H_2O$ (KLD-3).

A solution of $C_6H_5PO_3H_2$ (0.040 g, 0.25 mmol) and $CoCl_2$ (0.130 g, 1.00 mmol) in 5 mL of 1 M LiCl was added dropwise to a solution of **K-P_2W_{12}** (0.394 g, 0.1 mmol) in 15 mL of 1 M LiCl acidified by 50 μL glacial acetic acid under vigorous stirring. The pH of the resulting mixture was adjusted to 3.0 by addition of glacial acetic acid. The reaction solution was then placed in an oven and heated at 60 °C for 2 days. After cooling down to room temperature, 1 M aqueous solution of $[(CH_3)_2NH_2]Cl$ (30 drops) was added to the reaction mixture and it was left for evaporation. Transparent red block-like crystals of **KLD-3** form within 2 – 3 weeks. The crystals were collected by filtration and dried in air. Yield: 0.025 g (6.8 % based on {P}). Elemental analysis: calculated for $C_{21}H_{128}Co_3K_2Li_{1.5}N_{4.5}O_{134}P_6W_{24}$ (found), mass %: C, 3.38 (3.27); H, 1.73 (1.74); K, 1.05 (1.06); Li, 0.14 (0.15); N, 0.85 (0.90); Co, 2.37 (2.38); P, 2.49 (2.43); W, 59.21 (59.1) %. IR spectrum (KBr pellet), cm^{-1}: 3411 (s, br); 1621 (m); 1464 (w); 1438 (w); 1404 (w); 1157 (m); 1126 (m); 1085 (m); 1020 (m); 991 (m); 933 (s); 916 (s); 802 (s); 694 (s); 569 (m); 544 (m); 463 (m).

II. Single-crystal diffraction data for **KLD-1**, **KLD-2** and **KLD-3** were collected on a SuperNova (Agilent Technologies) diffractometer with MoKα radiation (λ = 0.71073 Å) at 120 K. The crystals were mounted in a Hampton cryoloop with Paratone-N oil to prevent water loss. Absorption corrections was applied numerically based on multifaceted crystal model using CrysAlis software.[2] The SHELXTL software package[3] was used to solve and refine the structure. The structures were solved by direct methods and refined by full-matrix least-squares method against $|F|^2$ with anisotropic thermal parameters for all heavy atoms (W, Co, P, As and K). Hydrogen atoms of the phenyl rings were placed in geometrically calculated positions. Hydrogen atoms of the disordered solvent molecules as well as DMA^+ countercations were not located.

The relative site occupancy factors for the disordered positions of Co(1) ions in **KLD-3** as well as potassium, oxygen, carbon and nitrogen atoms of co-crystallized water molecules and counterions in all the three structures were first refined in an isotropic approximation with U_{iso}= 0.05 and then fixed at the obtained values and refined without the thermal parameters restrictions.

Due to severe disorder we could only locate 3 DMA^+ cations in the structure of **KLD-1**, 1.5 DMA^+ cations in the structure of **KLD-2** and 3.5 DMA^+ cations in the structure of **KLD-3**, while 4.5 counterions per formula unit were found for each of the three compounds by elemental analysis.

Similarly, only 9.25, 11 and 8.25 heavily disordered oxygen atoms of co-crystallized water molecules could be located in the crystal structures of **KLD-1**, **KLD-2** and **KLD-3**, respectively, that can be compared with 35, 40 and 28 solvent H_2O molecules found for these compounds by combination of elemental and thermogravimetrical analyses. This is consistent with the large solvent-accessible volume remaining in the structures. For the overall consistency, the final formulae in the CIFs correspond to the composition of the bulk materials determined by elemental analysis and TGA.

The rather high value of R_{int} for **KLD-1** (0.17) combined with several violations of systematic absences is consistent with the twinning issue. The application of (−1, 0, 0; 0, −1, 0; 0, 0, −1) twinning low allowed slightly improve R_1 and other parameters (BASF 0.48).

Additional crystallographic data are summarized in Table S1. Further details on the crystal structures investigation can be obtained, free of charge, on application to CCDC, 12 Union Road, Cambridge CB2 1EZ, UK: http://www.ccdc.cam.ac.uk, e-mail: data_request@ccdc.cam.ac.uk, or fax: +441223 336033 upon quoting 1586966 (**KLD-1**), 1586967 (**KLD-2**) and 1586968 (**KLD-3**) numbers. The main bond lengths and angles in **1** – **2** are shown in Table S2.

Table S1. Crystal data and structure refinement details for **KLD-1**, **KLD-2** and **KLD-3**

Sample	**KLD-1**	**KLD-2**	**KLD-3**
Empirical formula	$C_{21}H_{116}K_{3.5}Li_8N_{4.5}O_{129}P_6W_{24}$	$C_{21}H_{126}As_2K_{3.5}Li_8N_{4.5}O_{134}P_4W_{24}$	$C_{21}H_{128}Co_3K_2Li_{1.5}N_{4.5}O_{134}P_6W_{24}$
Formula weight, g/mol	7286.77	7464.75	7451.90
Crystal system	Monoclinic	Monoclinic	Monoclinic
Space group	*C*2	*C*2	*C*2
a / Å	26.5106(18)	26.5613(17)	26.212(2)
b / Å	28.0247(4)	28.3926(4)	28.3669(6)
c / Å	14.2981(10)	14.2563(9)	14.1580(11)
β	140.094(14)°	140.272(13)°	140.132(16)°
Volume / Å^3	6814.9(7)	6871.6(6)	6748.2(7)
Z	2	2	2
D_{calc}, g/cm^3	3.551	3.608	3.667
Absorption coefficient, mm^{-1}	20.460	20.750	20.976
F(000)	6524	6696	6694
Crystal size, mm^3	0.12 × 0.18 × 0.23	0.12 × 0.23 × 0.25	0.11 × 0.15 × 0.22
Theta range for data collection	4.20° – 25.02°	4.18° – 26.02°	4.19° – 25.68°
Completeness to Θ_{max}	94.6 %	99.5 %	99.5 %
Index ranges	–30 < *h* < 31, –33 < *k* < 33, –17 < *l* < 16	–32 < *h* < 32, –35 < *k* < 35, –17 < *l* < 17	–31 < *h* < 31, –34 < *k* < 34, –17 < *l* < 17
Reflections collected	31084	34786	33510
Independent reflections	10447	13220	11559
R_{int}	0.1696	0.0575	0.0657
Observed ($I > 2\sigma(I)$)	8832	10996	10317
Absorption correction	Numerical based on gaussian integration over a multifaceted crystal model		
T_{min} / T_{max}	0.0311 / 0.2019	0.0280 / 0.1813	0.0187 / 0.2083
Data / restraints / parameters	10447 / 19 / 419	13220 / 19 / 470	11559 / 13 / 476
Goodness-of-fit on F^2	1.041	1.023	1.051
R_1, wR_2 ($I > 2\sigma(I)$)	R_1 = 0.0717, wR_2 = 0.1753	R_1 = 0.0483, wR_2 = 0.1132	R_1 = 0.0422, wR_2 = 0.0962
R_1, wR_2 (all data)	R_1 = 0.0848, wR_2 = 0.1917	R_1 = 0.0655, wR_2 = 0.1268	R_1 = 0.0509, wR_2 = 0.1034
Largest diff. peak and hole / e Å^{-3}	4.331 / –3.755	1.524 / –1.233	2.806 / –1.921

Table S2. Selected bond lengths (Å) and angles (°) in **1** and **2** as determined from the crystal structure of **KLD-1** and **KLD-2**.

KLD-1		**KLD-2**	
Bond type	***Length***	***Bond type***	***Length***
P_L–O_t	1.54(3)	As–O_t	1.65(2)
P_L–μ_2-O (W–O–P_L)	1.53(3)–1.59(3)	As–μ_2-O (W–O–As)	1.675(18)–1.714(16)
P_L–C	1.796(16)	As–C	1.874(11)
P–O	1.50(2)–1.62(3)	P–O	1.510(14)–1.593(16)
W=O_t	1.65(3)–1.78(2)	W=O_t	1.704(15)–1.773(15)
W–μ_2-O (W–O– P_L)	2.09(2)–2.09(3)	W–μ_2-O (W–O–As)	2.053(18)–2.072(16)
W–μ_2-O (W–O–P)	2.086(17)–2.13(2)	W–μ_2-O (W–O–P)	2.122(12)–2.138(13)
W–μ_2-O (W–O–W)	1.73(3)–2.12(2)	W–μ_2-O (W–O–W)	1.740(16)–2.132(14)
W–μ_3-O (2 W + P)	2.20(2)–2.30(2)	W–μ_3-O (2 W + P)	2.232(15)–2.312(13)
Angle type	***Angle value***	***Angle type***	***Angle value***
O-P_L-O	108.0(15)–112.1(15)	O-As-O	105.9(9)–110.6(9)
O- P_L-C	106.3(15)–111.6(12)	O-As-C	108.3(9)–112.3(8)

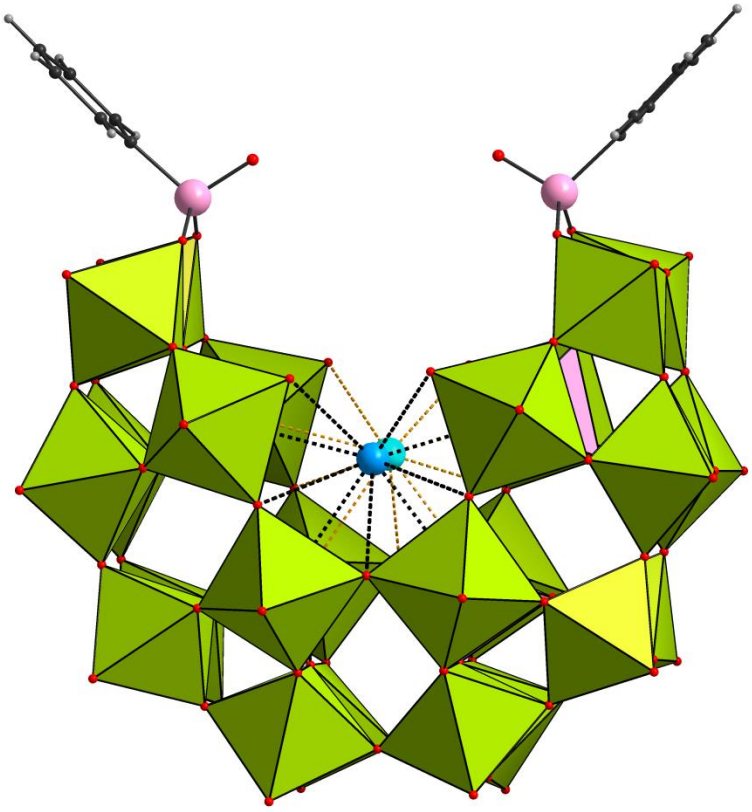

Figure S1. Structure of polyanions $[K\subset(C_6H_5XO)_2P_4W_{24}O_{92}]^{15-}$ in **KLD-1** and **KLD-2**. WO_6: lime green octahedra, PO_4: pink tetrahedra; As/P: pink, C: black, H: gray, O: red spheres. Two equally occupied (50 %) positions (blue/light blue) of the K^+ ion in the central cavity of the POM are shown with black/orange dashed K–O bonds.

III. Bond valence sum calculations

Bond valence sum calculations[4] for **KLD-1** (Table S3), **KLD-2** (Table S4) and **KLD-3** (Table S5) are consistent with the oxidation state +VI for all W centers and +V for all P and As centers in **1** – **3**, and +II for the Co centers in **3**. The BVS values for the oxygen atoms suggest that there is no protonation of any oxygen positions in the POM skeleton of the polyanions **1** – **3**, while the terminal oxygens coordinated to Co^{II} ions in **3** belong to aqua ligands.

Table S3. Bond valence sum values for different atoms in **KLD-1**

W and P centers		O6T	–1.56	**μ_2-O (W–O–W)**	
W1	6.40	O6	–1.61	O12	–1.90
W2	6.52	O7T	–1.53	O13	–2.06
W3	6.17	O8T	–2.04	O14	–2.03
W4	6.58	O9T	–1.72	O25	–2.13
W5	6.12	O10T	–1.93	O26	–2.09
W6	6.34	O11T	–1.95	O34	–1.98
W7	6.29	O12T	–1.90	O37	–2.20
W8	6.72	**Terminal oxygens of P_L=O**		O45	–1.84
W9	6.28	O3P3	–1.28	O48	–2.16
W10	6.42	**μ_2-O (W–O–P_L)**		O56	–1.95
W11	6.29	O1P3	–2.06	O59	–2.21
W12	6.35	O2P3	–1.84	O78	–2.07
P1	4.73	**μ_2-O (W–O–P)**		O89	–1.91
P2	4.62	O2P1	–2.04	O102	–2.08
P3	4.41	O4P1	–1.90	O112	–2.15
Terminal oxygens of W=O		O1P2	–1.83	O121	–1.95
O1T	–1.83	O3P2	–1.83	O610	–2.22
O2T	–1.84	**μ_3-O (2W+P)**		O710	–2.17
O3	–1.68	O1P1	–1.91	O711	–2.11
O3T	–1.54	O3P1	–1.97	O811	–2.20
O4T	–2.06	O2P2	–1.97	O910	–2.11
O5T	–1.69	O4P2	–1.94	O912	–2.05

Table S4. Bond valence sum values for different atoms in **KLD-2**

W, P and As centers		O6T	–1.53	**μ_2-O (W–O–W)**	
W1	6.20	O6	–1.55	O12	–2.00
W2	6.41	O7T	–1.77	O13	–2.06
W3	6.36	O8T	–1.73	O14	–2.07
W4	6.10	O9T	–1.59	O25	–2.08
W5	6.11	O10T	–1.78	O26	–2.10
W6	6.03	O11T	–1.81	O34	–1.89
W7	6.44	O12T	–1.85	O37	–2.18
W8	6.09	**Terminal oxygens of As=O**		O45	–1.88
W9	5.99	O3A1	–1.45	O48	–2.14
W10	6.33	**μ_2-O (W–O–As)**		O56	–1.98
W11	6.32	O1A1	–2.12	O59	–2.13
W12	6.28	O2A1	–1.92	O78	–2.05
P1	4.80	**μ_2-O (W–O–P)**		O89	–1.77
P2	4.89	O2P1	–1.97	O102	–2.10
As1	4.83	O4P1	–1.92	O112	–2.10
Terminal oxygens of W=O		O1P2	–1.88	O121	–1.88
O1T	–1.81	O3P2	–1.85	O610	–2.21
O2T	–1.82	**μ_3-O (2W+P)**		O710	–2.17
O3T	–1.65	O1P1	–1.88	O711	–2.09
O3	–1.64	O3P1	–1.95	O811	–2.03
O4T	–1.66	O2P2	–2.05	O910	–2.10
O5T	–1.58	O4P2	–1.91	O912	–2.01

Table S5. Bond valence sum values for different atoms in **KLD-3**

W, P and Co centers		O9T	–1.84	O34	–2.05
W1	6.37	O10T	–1.78	O37	–2.19
W2	6.21	O11T	–1.89	O45	–1.93
W3	6.36	O12T	–1.82	O48	–2.15
W4	6.30	**Terminal oxygens of P_L=O**		O56	–1.98
W5	6.28	O3P3	–1.63	O59	–2.15
W6	6.39	**Terminal oxygens of Co–O_{H2O}**		O78	–2.09
W7	6.26	O11C	–0.18	O89	–1.96
W8	6.09	O12C	–0.19	O102	–2.14
W9	5.26	O13C	–0.12	O112	–2.14
W10	6.40	O14C	–0.14	O121	–1.96
W11	6.38	O21C	–0.36	O610	–2.17
W12	6.43	O22C	–0.32	O710	–2.15
P1	4.98	O23C	–0.39	O711	–2.10
P2	4.94	O24C	–0.35	O811	–2.01
P3	4.84	**μ_2-O (W–O–P_L)**		O910	–2.07
Co1	1.98	O1A1	–1.97	O912	–1.99
Co2	2.06	O2P3	–1.95	**μ_2-O (W–O–P)**	
Terminal oxygens of W=O		**μ_2-O (Co–O–W)**		O2P1	–1.95
O1T	–1.72	O3C1	–1.92	O4P1	–1.91
O2T	–1.71	O6C1	–1.91	O1P2	–1.93
O3T	–1.62	**μ_2-O (W–O–W)**		O3P2	–1.91
O4T	–1.94	O12	–2.03	**μ_3-O (2W+P)**	
O5T	–1.97	O13	–2.08	O1P1	–1.97
O6T	–1.68	O14	–2.12	O3P1	–1.93
O7T	–1.72	O25	–2.04	O2P2	–1.95
O8T	–1.70	O26	–2.06	O4P2	–1.90

IV. Thermal analysis

TGA measurements were performed from 25 °C to 950 °C under N_2 atmosphere. According to the obtained data the thermal decomposition of **KLD-1** and **KLD-2** proceeds in a similar way and involves three main steps of weight loss (Fig. S1, S2 and S3, respectively). The first step occurring in the temperature range of 25 – 270 °C for **KLD-1,** 25 – 255 °C for **KLD-2** and 25 – 250 °C for **KLD-3** is characteristic to the release of 35 (8.65 % calc. *vs*. 8.42 % obs. for **KLD-1**) and 40 (9.65 % calc. *vs*. 10.06 % obs. for **KLD-2**) lattice water molecules as well as 28 lattice water molecules accompanying 12 coordinated water molecules for **KLD-3** (8.94 % calc. *vs*. 9.28 % obs.) per formula unit. The next step of the weight loss corresponds to the decomposition and removal of phenyl groups in **1** - **3** as well as DMA^+ counterions (4.92 % calc. *vs*. 4.21 % obs. for **KLD-1** (270 – 825 °C), 4.81 % calc. *vs*. 5.34 % obs. for **KLD-2** (255 – 730 °C) and 4.88 % calc. *vs*. 4.08 % obs. for **KLD-3** (250 – 850 °C). The mass loss at higher temperatures could be attributed to decomposition of the POT skeleton as well as As volatility for **KLD-2** (e.g. in the form of As_4O_6). Accordingly, the total loss of the mass at 900 °C constitutes 17.41 % for **KLD-1**, 22.81 % for **KLD-2** and 17.45% for **KLD-3**.

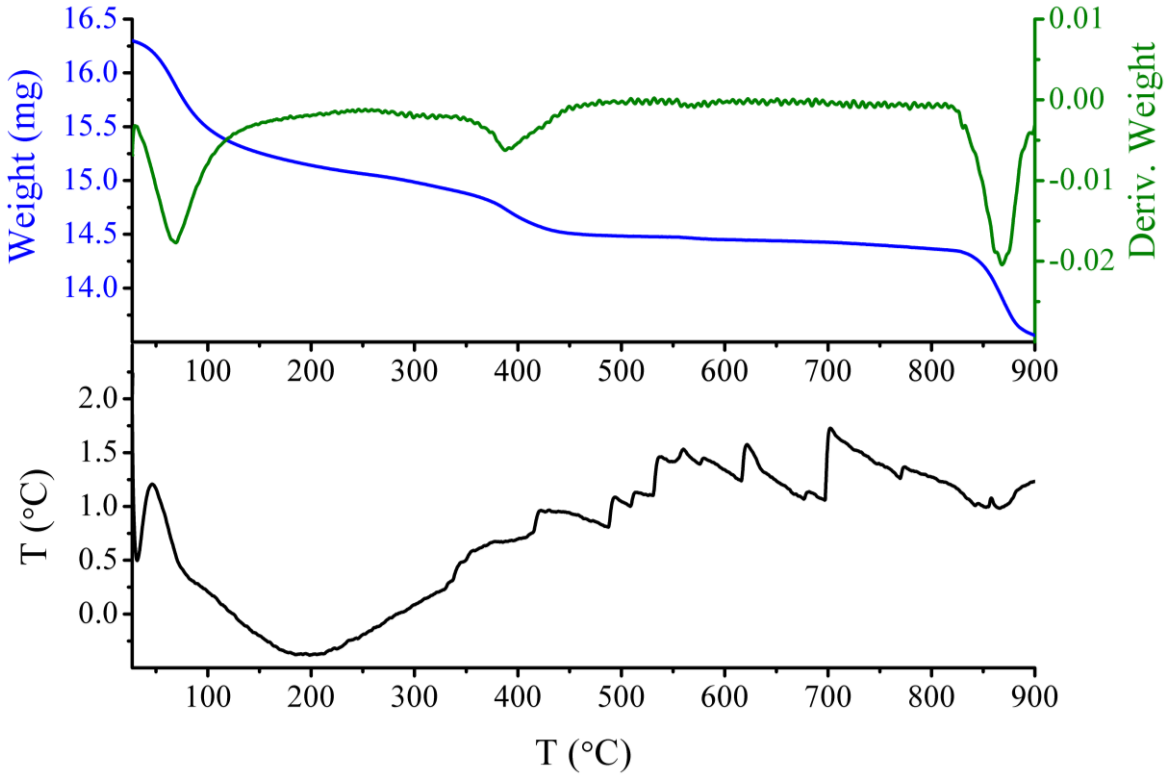

Figure S2. TGA (blue), differential TGA (green) and SDTA (black) curves for **KLD-1** from room temperature to 900 °C under N_2 atmosphere.

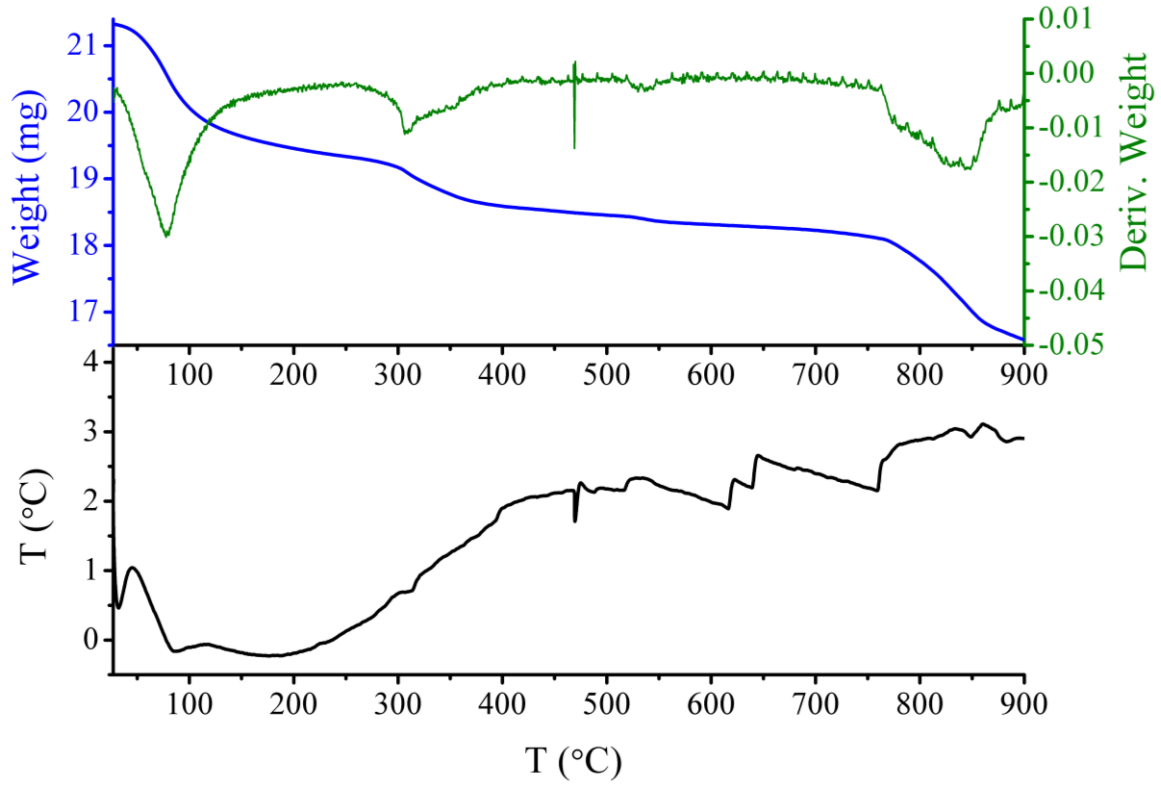

Figure S3. TGA (blue), derivative TGA (green) and SDTA (black) curves for **KLD-2** from room temperature to 900 °C under N_2 atmosphere.

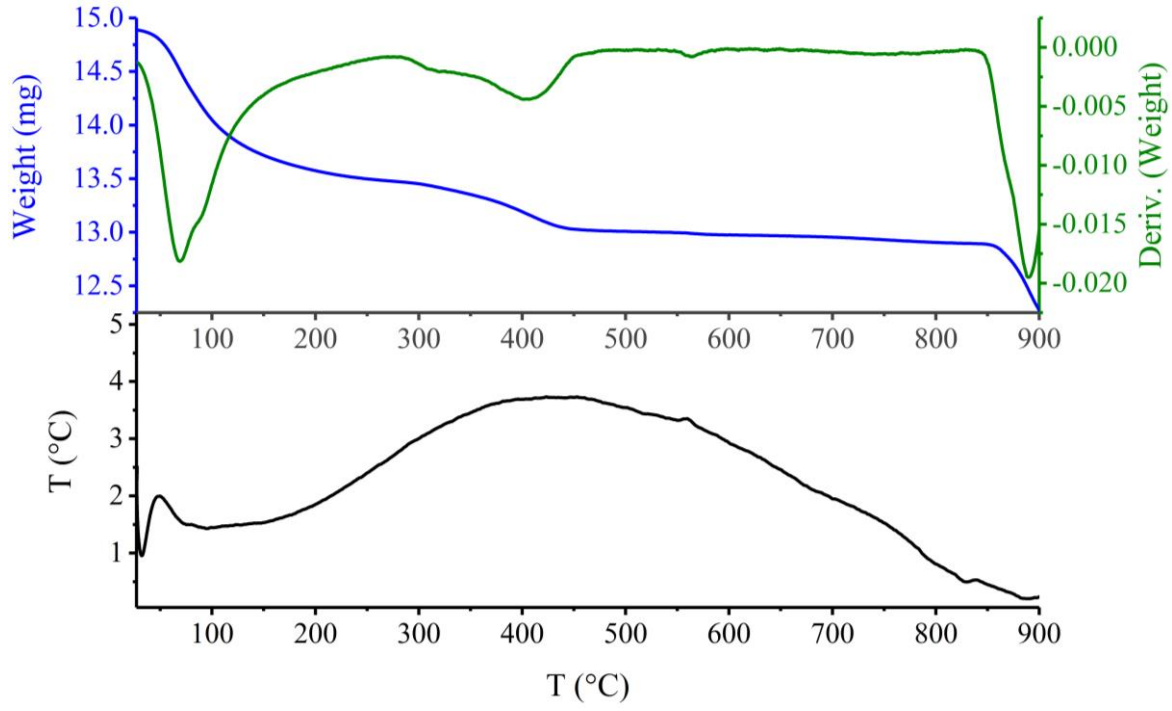

Figure S4. TGA (blue), derivative TGA (green) and SDTA (black) curves for **KLD-3** from room temperature to 900 °C under N_2 atmosphere.

V. Vibrational spectra

The IR spectra of **KLD-1** and **KLD-2** were recorded between 4000 and 375 cm^{-1} as KBr pellets and exhibit some distinct features consistent with the crystal structures of these compounds (Fig. S4). Thus, the IR spectrum of the **K-P_2W_{12}** precursor exhibit four bands at 1130, 1082, 1010, 972 cm^{-1} characteristic for stretching vibrations of P–O bonds. In the spectra of **KLD-1** and **KLD-2** these bands are shifted to 1161, 1128, 1088, 1020, 989 cm^{-1} and 1161, 1086, 1018, 989 cm^{-1}, respectively, reflecting dimerization of the $\{P_2W_{12}\}$ units and coordination of $C_6H_5XO_3^{2-}$ ligands in **1** and **2**. The spectrum of **KLD-1** exhibits two additional peaks centered at 1128 and 974 cm^{-1} which should correspond to stretching vibrations of P–C and P–O in the $C_6H_5PO_3^{2-}$ groups, respectively. Additional vibrations bands of P–C and As–C bonds appear at around 550 – 525 cm^{-1} and overlap with vibration of POT skeleton in **1** and **2**. The characteristic range for As–O vibrations usually constitutes 880 – 700 cm^{-1},[5] therefore the unique band at 785 cm^{-1} in the spectrum of **KLD-2**, which is not present in the spectrum of **KLD-1** should most likely belong to As–O vibrations of phenylarsonate ligands in **1**.

The bands at around 929 and 916 cm^{-1} (both compounds) could be attributed to vibrations of W=O bands and could be compared with the peak at 910 cm^{-1} in the spectrum of K-P_2W_{12}. Further pronounced differences in the spectra of the precursor salt and **KLD-1** / **KLD-2**, reflecting P_2W_{12} dimerization and ligand attachment appear in the region of 900 – 500 cm^{-1} characteristic for W–O–W, W–O–P and W–O–As vibrations.

The weak bands at around 1466 and 1440 cm^{-1} reflect vibrations of C–C bonds of the $C_6H_5PO_3^{2-}$ (**KLD-1**)or $C_6H_5AsO_3^{2-}$ (**KLD-2**) ligands as well as C–N bonds of DMA^+ counterions. The broad peak centered at 3432 for **KLD-1** and 3426 cm^{-1} for **KLD-2** as well as the signal at 1631 (**KLD-1**) or 1629 cm^{-1} (**KLD-2**) belong to symmetrical and asymmetrical vibrations of co-crystallized water molecules, respectively.

The spectrum of **KLD-3** is very similar to that of **KLD-1** (Fig. S6) with only minor shifts of some bands, reflecting the structural similarities of the both compounds.

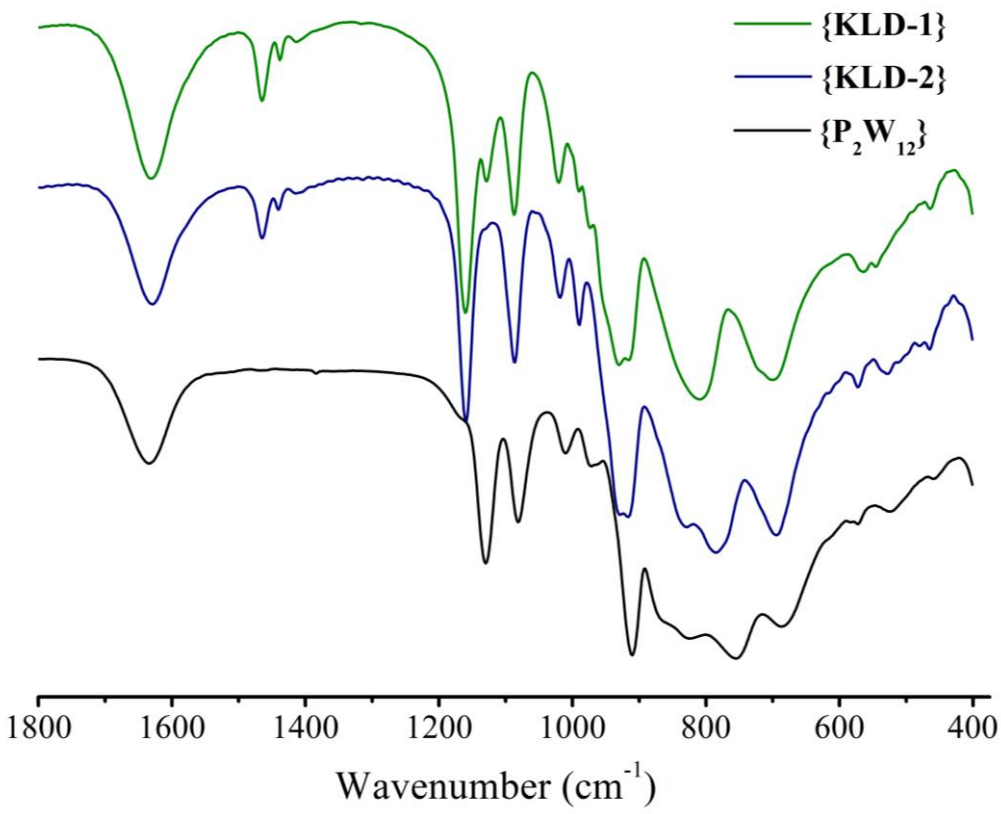

Figure S5. FT-IR spectra of **KLD-1** (green) and **KLD-2** (navy) in comparison with that of the **K-P_2W_{12}** precursor (black)

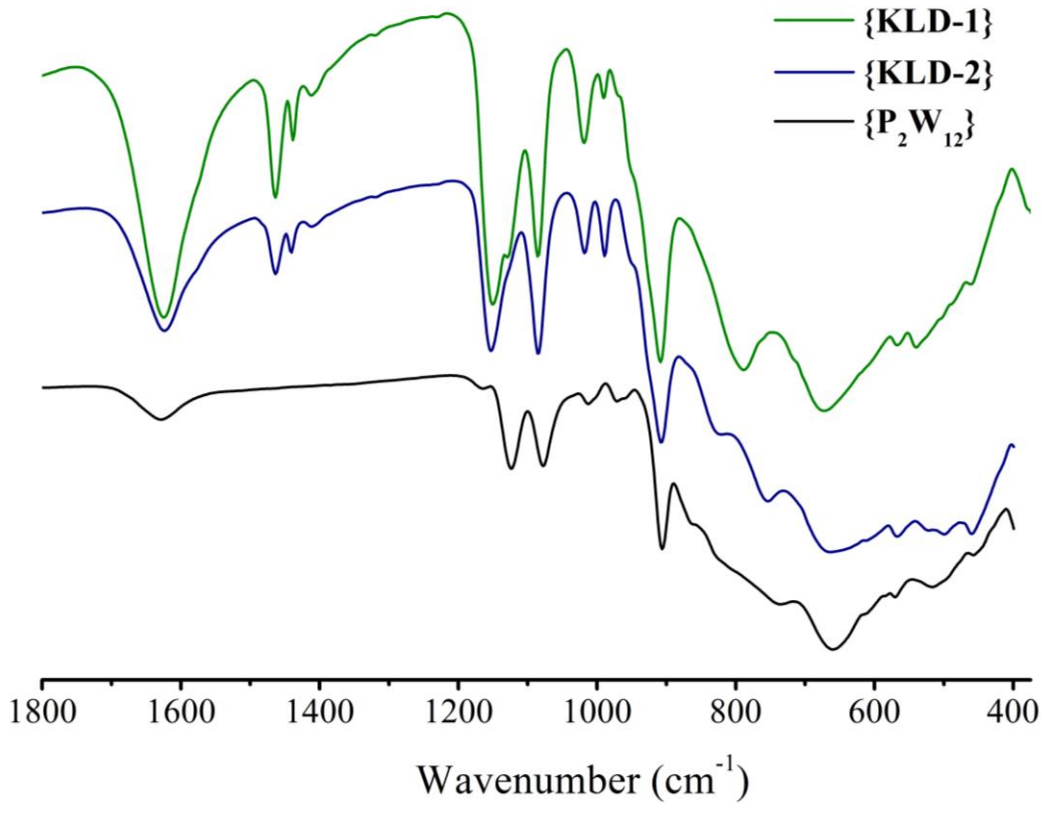

Figure S6. Diamond ATR FT-IR spectra of **KLD-1** (green) and **KLD-2** (navy) in comparison with that of the **K-P_2W_{12}** precursor (black)

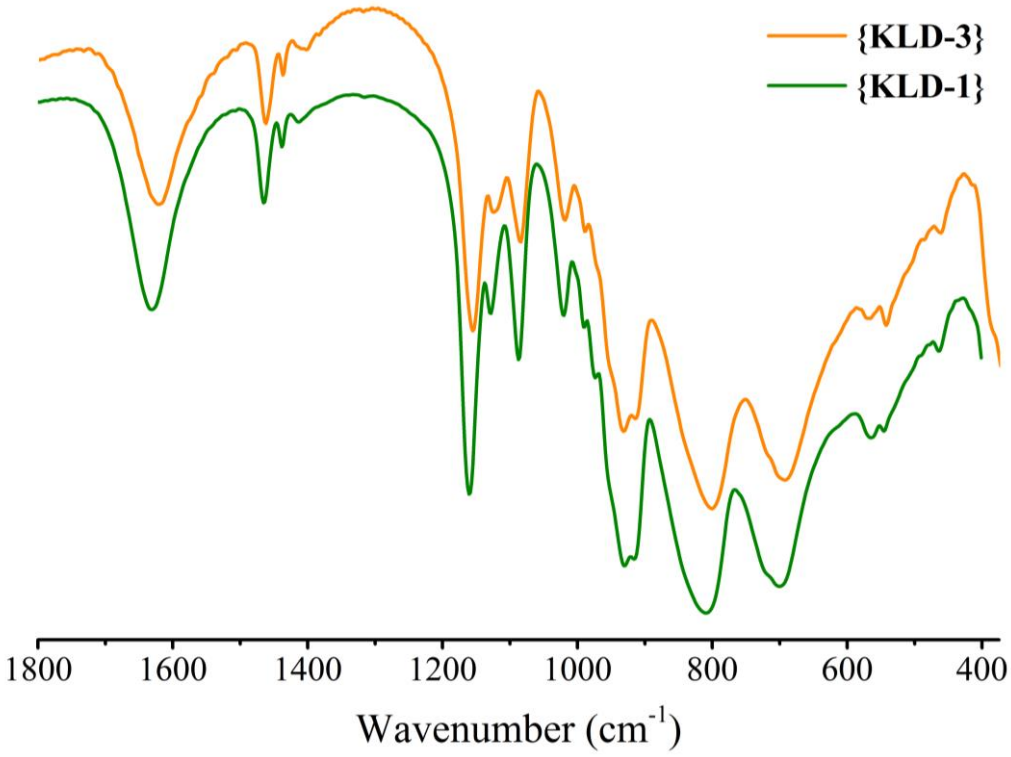

Figure S7. FT-IR spectrum of **KLD-3** (orange) in comparison with the spectrum of the **KLD-1** (green).

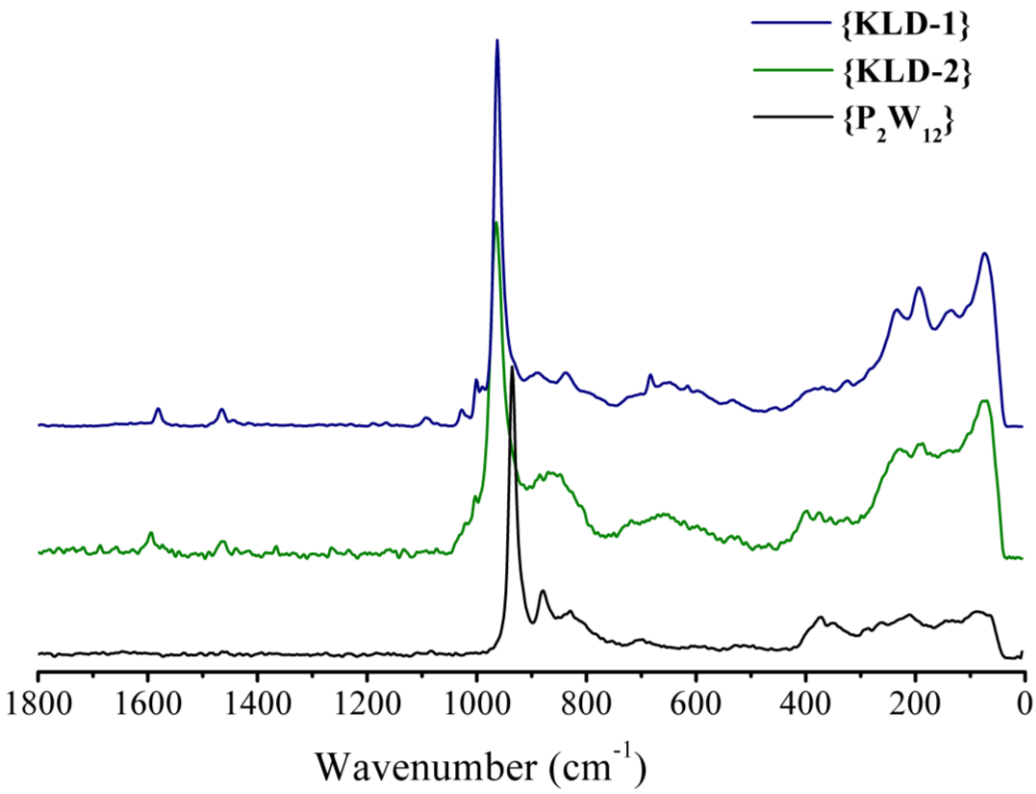

Figure S8. Raman spectra of **KLD-1** (navy) and **KLD-2** (green) in comparison with that of the **K-P_2W_{12}** precursor (black).

VI. ^{31}P NMR spectra

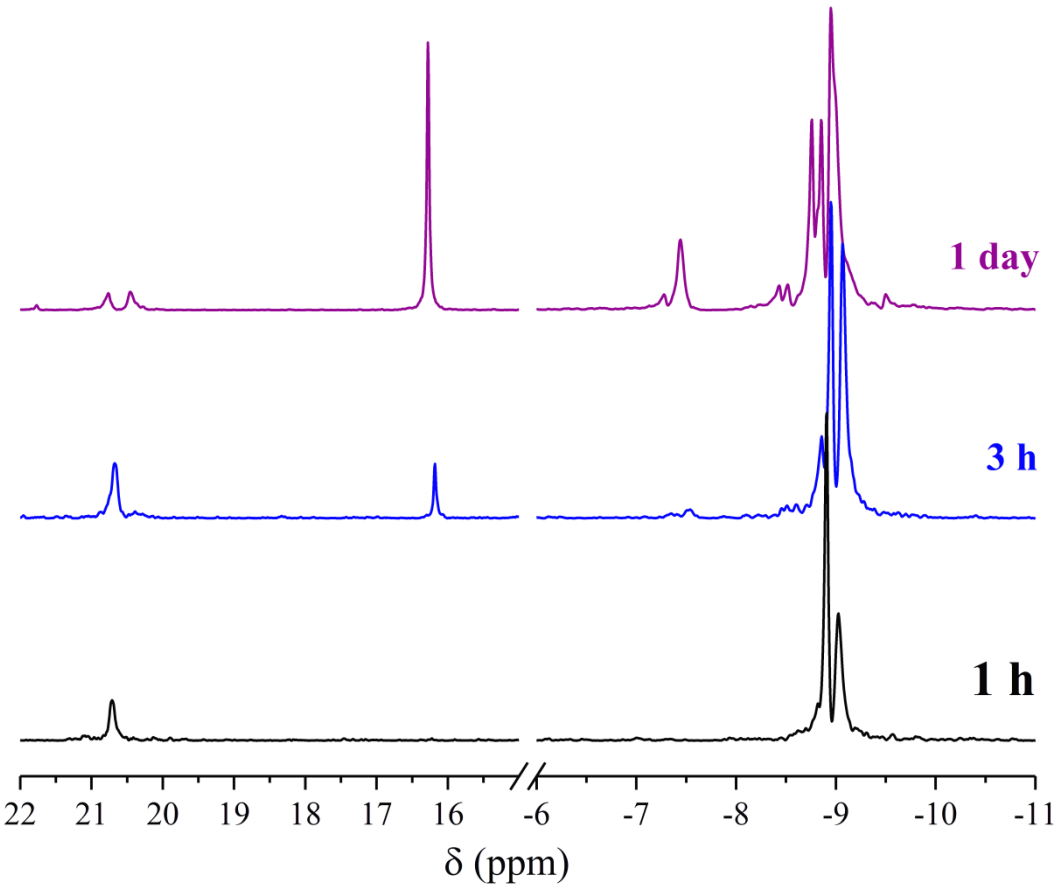

Figure S9. Room temperature ^{31}P NMR spectra of **KLD-1** dissolved in 1 M $LiCl_{aq}$ after 1 h (black line), after 1 day (blue line) and after 1 day (purple line).

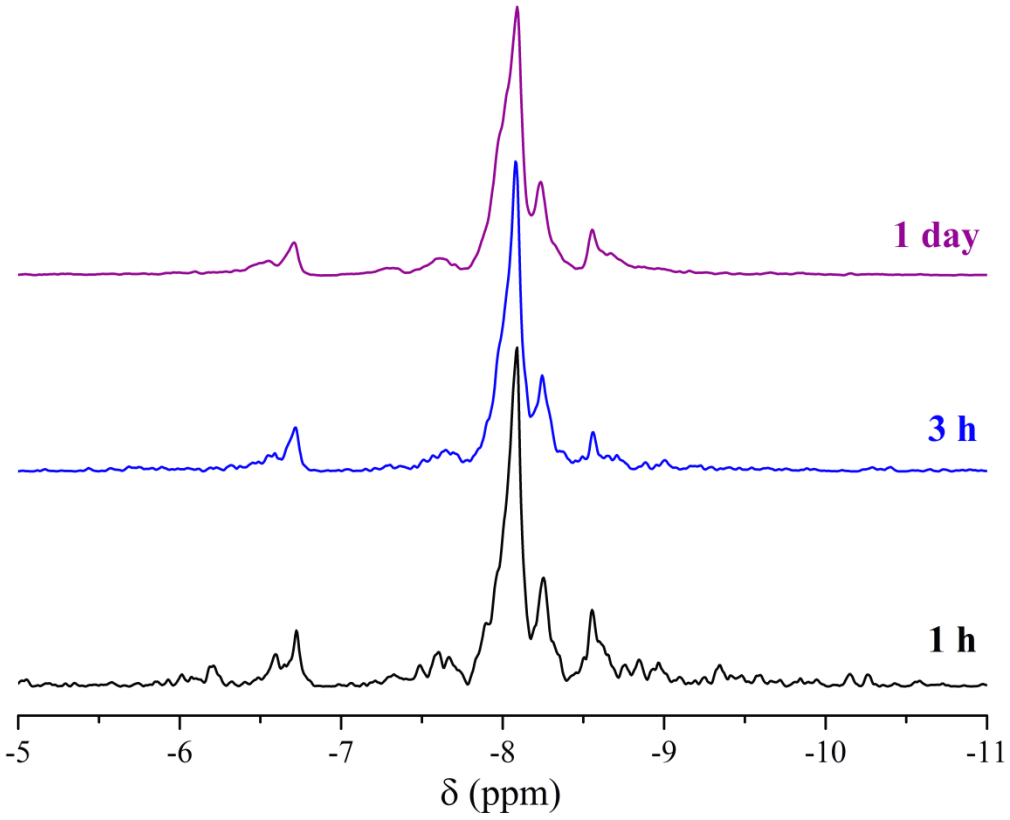

Figure S10. Room temperature ^{31}P NMR spectra of **KLD-2** dissolved in H_2O after 1 h (black line), after 1 day (blue line) and after 1 day (purple line).

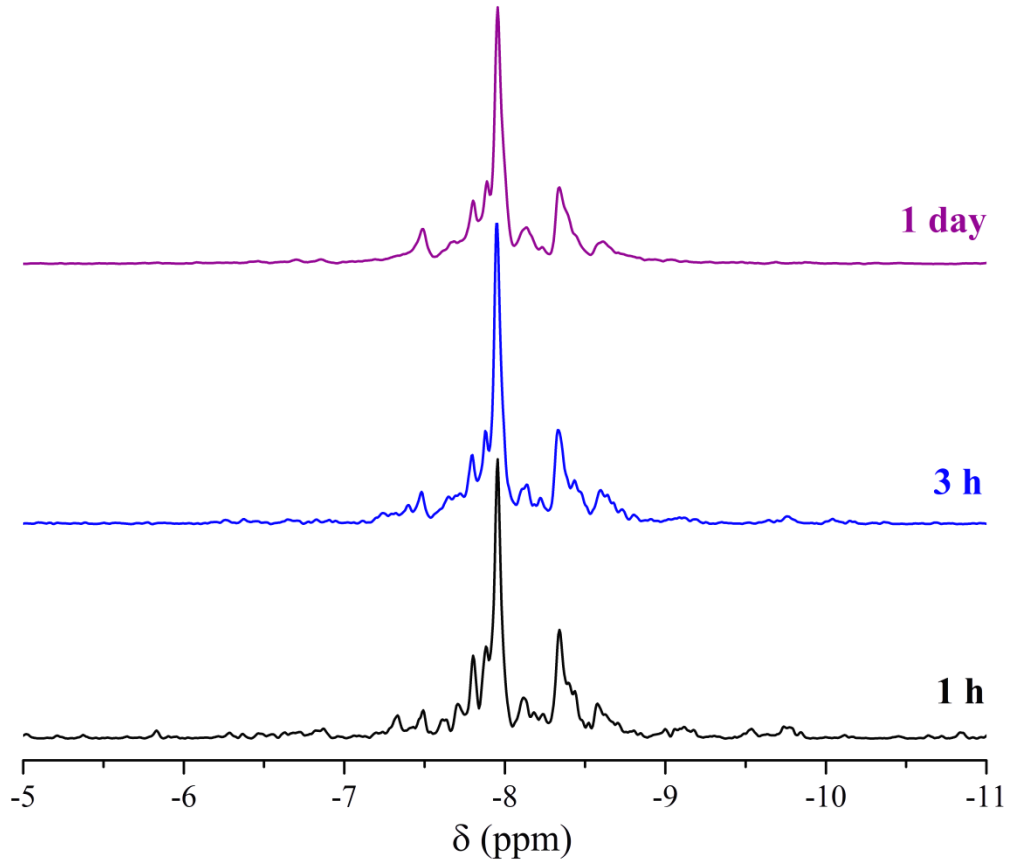

Figure S11. Room temperature ^{31}P NMR spectra of **KLD-2** dissolved in 1 M $LiCl_{aq}$ after 1 h (black line), after 1 day (blue line) and after 1 day (purple line).

VII. UV-Vis spectra

The UV-Vis spectra of **KLD-1** and **KLD-2** in 1 M aqueous LiCl solution show similar characteristics (Fig. S12 and S14, respectively). Two absorption maxima in these spectra, appearing at around 210 nm and 270 nm, are typical for the LMCT of pπ ($O_{terminal}$) → dπ* (W) electronic transitions in the W=O bonds and the dπ – pπ –dπ electronic transitions in the W–O–W bonds and could be also compared with the spectral characteristics of the free phenylphosphonate or phenylarsonate ligands (Fig. S12 and S14).

The spectra of **KLD-1** remain almost unchanged for one hour in a good agreement with the short-term stability of polyanions **1** in the same medium observed by ^{31}P NMR spectroscopy. Distinct changes in the light absorption pattern for the **KLD-1** solution occur within 3 h and become even more pronounced within 1 day (Fig. S13). The time-dependent UV-Vis measurements for **KLD-2** in 1 M $LiCl_{aq}$ (Fig. S15) exhibit noticeable changes in the absorption intensity already within 30 min and indicate fast POM decomposition. At that, the trend of the changes in the spectra of **2** is rather different from that obtained for **1** (compare Fig. S13 and S15), which could indicate different decomposition pathways for these polyanions in aqueous medium resulting in formation of different products, that would also be in line with our ^{31}P NMR observations (Fig. S9 and S11).

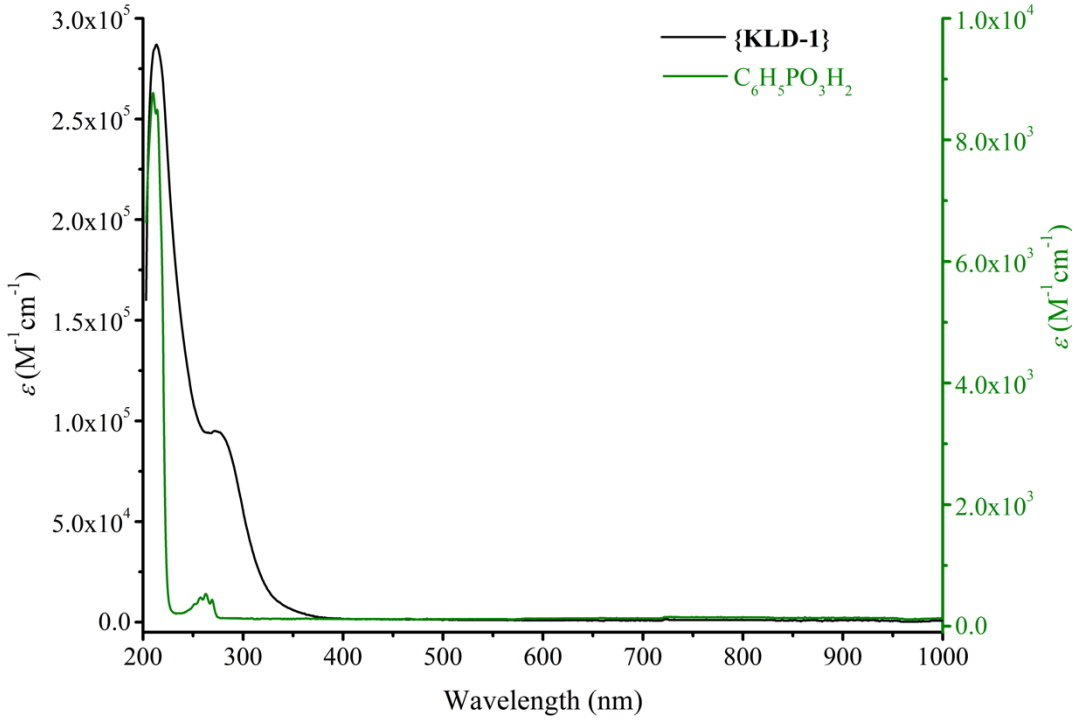

Figure S12. Room temperature UV-Vis spectrum of **KLD-1** in 1 M $LiCl_{aq}$ (black line; ε values are averaged from the spectra of the solution with the concentration between 2.27×10^{-6} M and 8.57×10^{-6} M) compared to the spectrum of $C_6H_5PO_3H_2$ in 1 M $LiCl_{aq}$ (green line; ε values are averaged from the spectra of the solution with the concentration between 7.91×10^{-5} M and 1.58×10^{-4} M).

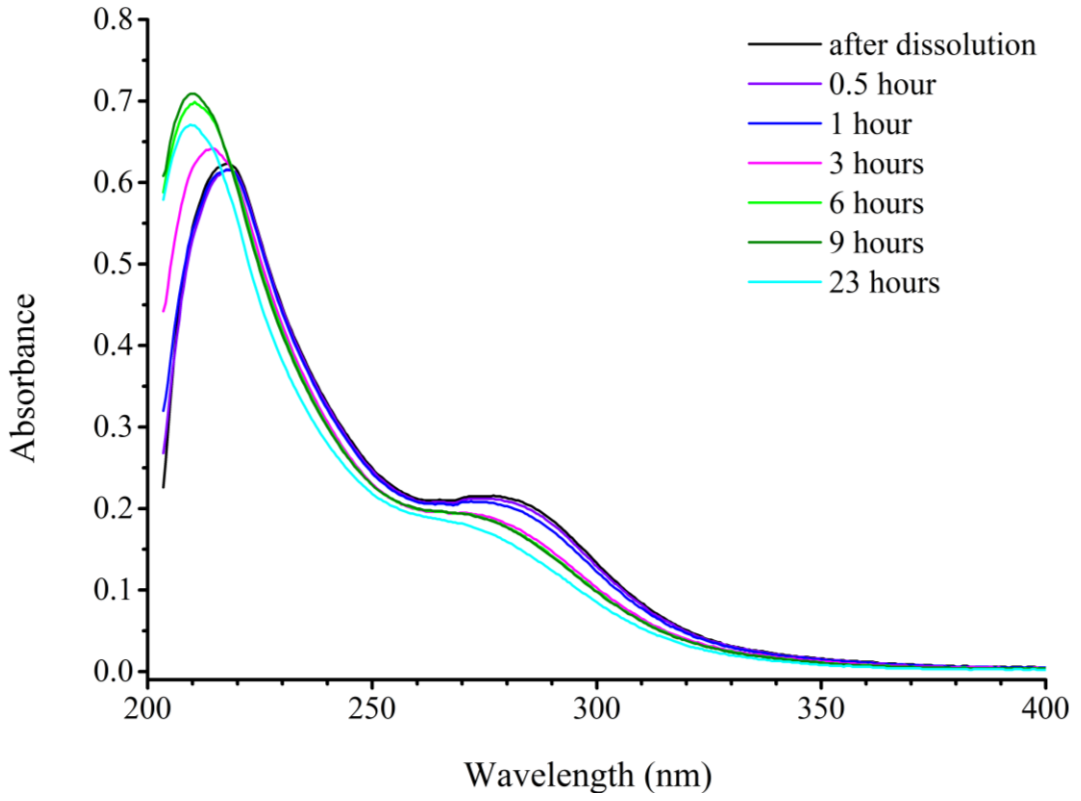

Figure S13. Time evolution of room temperature UV-Vis spectra of 2.27×10^{-6} M **KLD-1** solution in 1 M $LiCl_{aq}$.

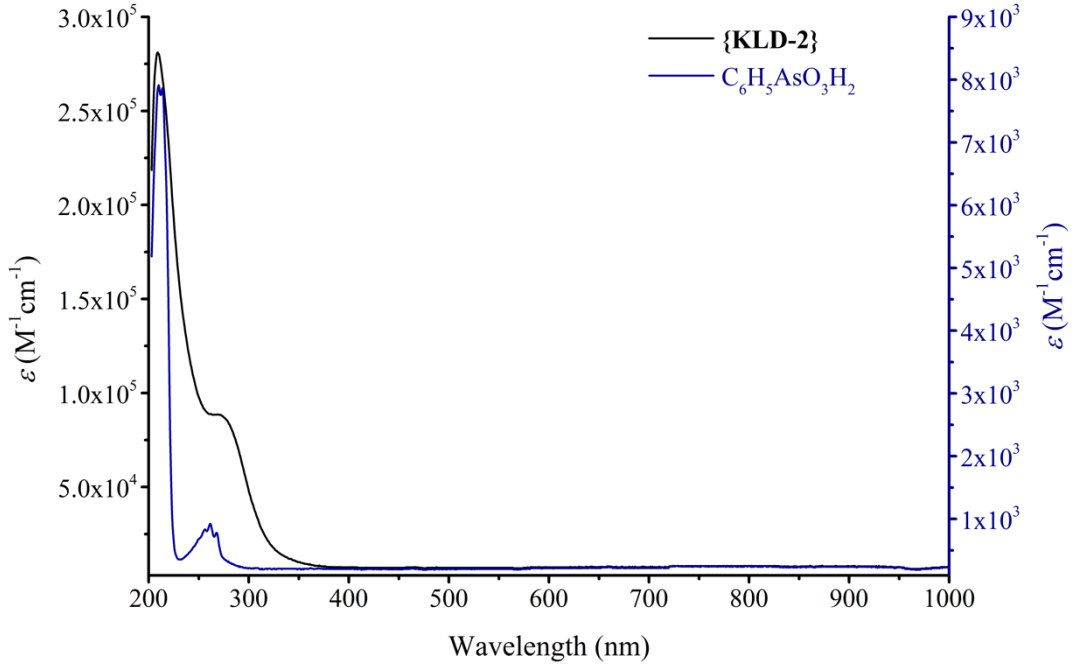

Figure S14. Room temperature UV-Vis spectrum of **KLD-2** in 1 M $LiCl_{aq}$ (black line; ε values are averaged from the spectra of the solution with the concentration between 2.26×10^{-6} M and 4.52×10^{-6} M, black) compared with the UV-Vis spectrum of $C_6H_5AsO_3H_2$ in 1 M $LiCl_{aq}$ (blue line; ε values are averaged from the spectra of the solution with the concentration between 6.19×10^{-5} M and 1.24×10^{-4} M, blue).

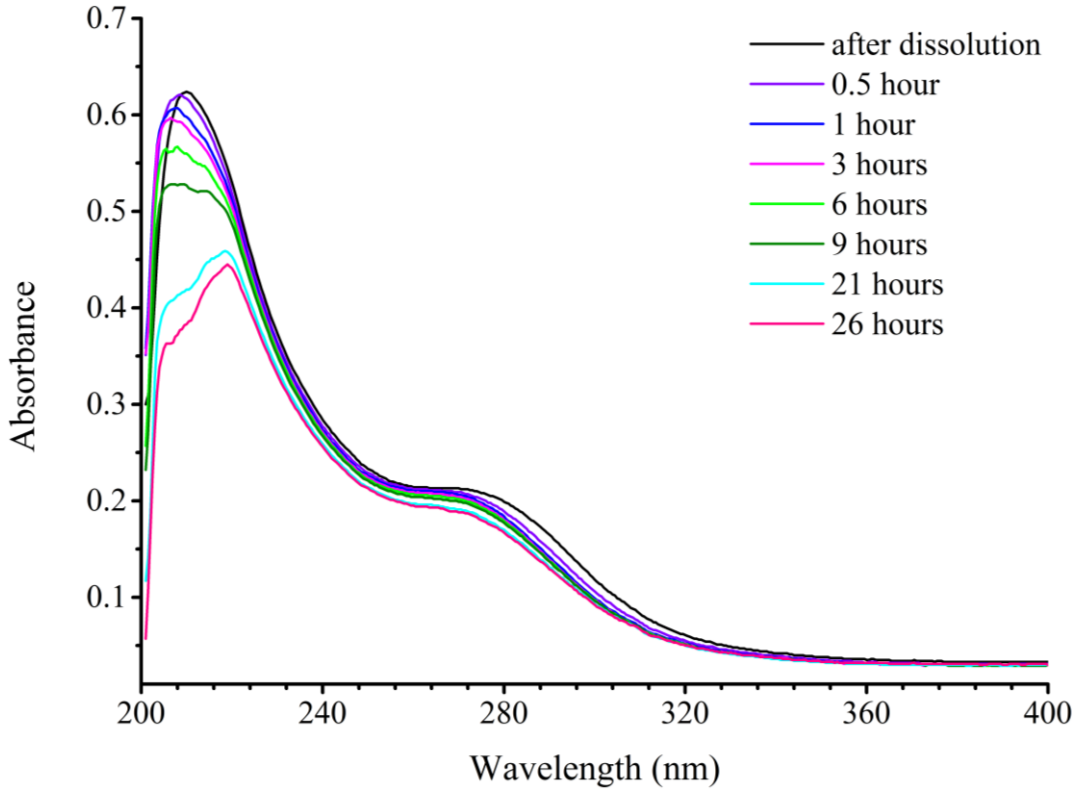

Figure S15. Time evolution of room temperature UV-Vis spectra of 2.26×10^{-6} M **KLD-2** solution in 1 M $LiCl_{aq}$.

VIII. Electrospray mass spectrometry measurements

Experimental details for the LC-ESI-FTICR-MS analysis. Analyses were performed using a hybrid linear ion trap FTICR mass spectrometer LTQ-FT (Thermo Fisher Scientific, Bremen, Germany) equipped with a 7 T superconducting magnet by infusion. The mass spectrometer was first tuned and calibrated in the negative mode following the standard optimization procedure for all voltages and settings. The complex was dissolved in 80 % H_2O and 20 % acetone. Mass spectra were recorded in full scan from 200 to 2000 Da with a resolution of 100.000 at *m*/*z* 400. All data were processed using the Xcalibur software version 2.1.

The complexity of the obtained spectrum allows attribution of the observed peaks to the ion pairs based on both intact $[(C_6H_5PO)_2P_4W_{24}O_{92}]^{16-}$ polyanions (see Figs. S16, S17) as well as on the species missing one phenylphosphonate group, $[(C_6H_5PO)P_4W_{24}O_{92}]^{18-}$ (Fig. S18) and Tables S6–S8.

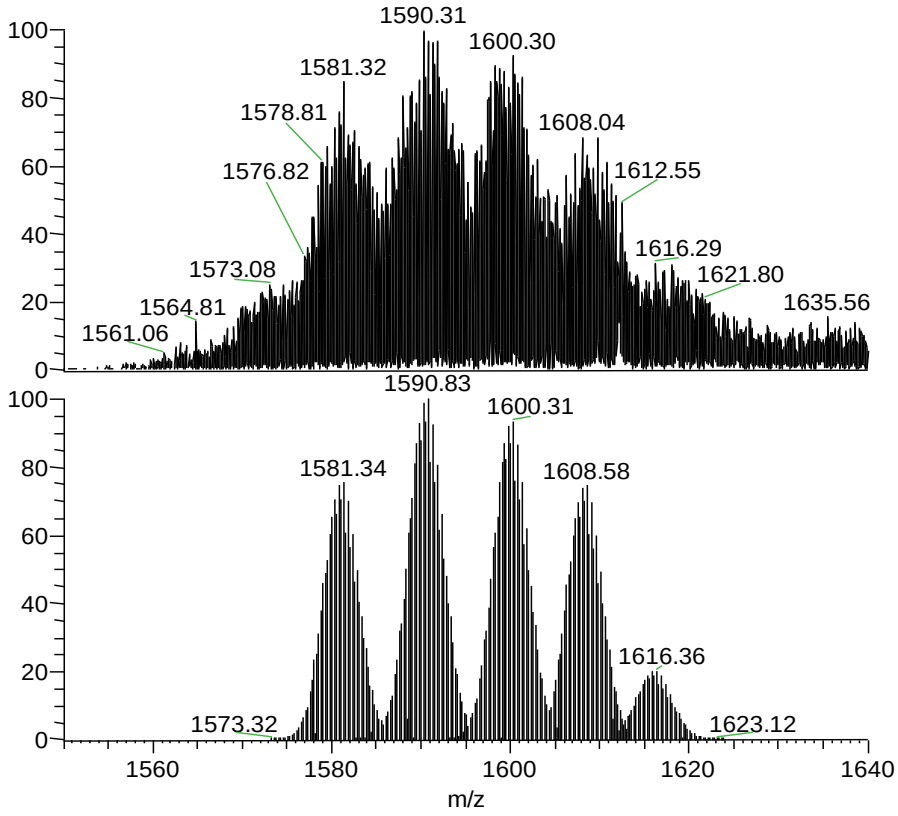

Figure S16. Comparison of the isotope distributions observed experimentally (upper part) and calculated for the –4 charged ion pairs based on the intact $[(C_6H_5PO)_2P_4W_{24}O_{92}]^{16-}$ polyanions (bottom). For the peak assignments see Table S6.

Table S6. Assignment of the signals from mass spectrometry (given as the value of the most abundant isotopologue) according to the simulation presented on Fig. S16.

Ion pair	*m*/*z* (calc)	Relative contribution to the simulated spectrum
$\{KLi_3H_8[(C_6H_5PO)_2P_4W_{24}O_{92}]\}^{4-}$	1581.34	0.70
$\{K_2Li_3H_7[(C_6H_5PO)_2P_4W_{24}O_{92}]\}^{4-}$	1590.83	1.00
$\{K_3Li_3H_6[(C_6H_5PO)_2P_4W_{24}O_{92}]\}^{4-}$	1600.31	1.00
$\{(DMA)K_3LiH_7[(C_6H_5PO)_2P_4W_{24}O_{92}]\}^{4-}$	1608.58	0.70
$\{(DMA)_2K_2Li_5H_3[(C_6H_5PO)_2P_4W_{24}O_{92}]\}^{4-}$	1616.36	0.25

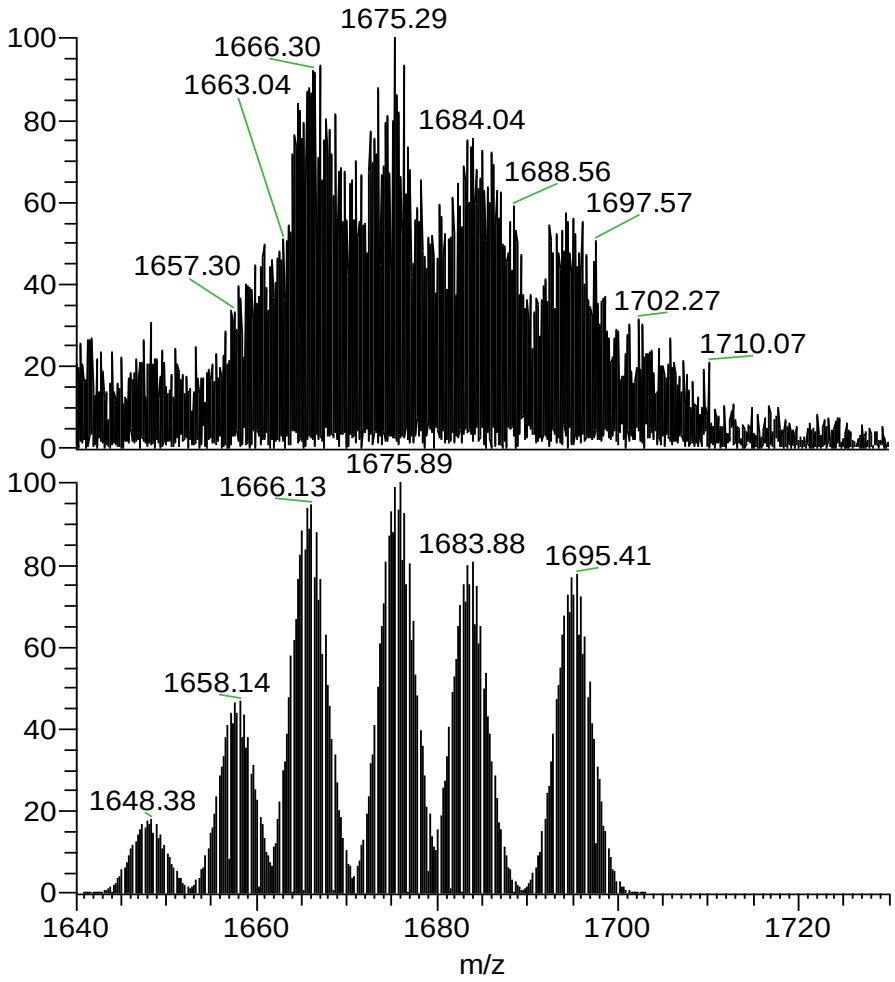

Figure S17. Comparison of the isotope splitting observed experimentally (upper part) and calculated for the –4 charged ion pairs based on $[(C_6H_5PO)_2P_4W_{24}O_{92}]^{16-}$ polyanions (bottom). For the peak assignments see Table S7.

Table S7. Assignment of the signals from mass spectrometry (given as the value of the most abundant isotopologue) according to the simulation presented on Fig. S17.

Ion pair	m / z (calc)	Relative contribution to the simulated spectrum
$\{(DMA)_4K_3Li_5[(C_6H_5PO)_2P_4W_{24}O_{92}]\}^{4-}$	1648.38	0.20
$\{(DMA)_5K_3Li_4[(C_6H_5PO)_2P_4W_{24}O_{92}]\}^{4-}$	1658.14	0.50
$\{(DMA)_5K_4Li_3[(C_6H_5PO)_2P_4W_{24}O_{92}]\}^{4-}$	1666.13	1.00
$\{(DMA)_6K_4Li_2[(C_6H_5PO)_2P_4W_{24}O_{92}]\}^{4-}$	1675.89	1.00
$\{(DMA)_6K_5Li[(C_6H_5PO)_2P_4W_{24}O_{92}]\}^{4-}$	1683.88	0.80
$\{(DMA)_8K_4[(C_6H_5PO)_2P_4W_{24}O_{92}]\}^{4-}$	1695.41	0.70

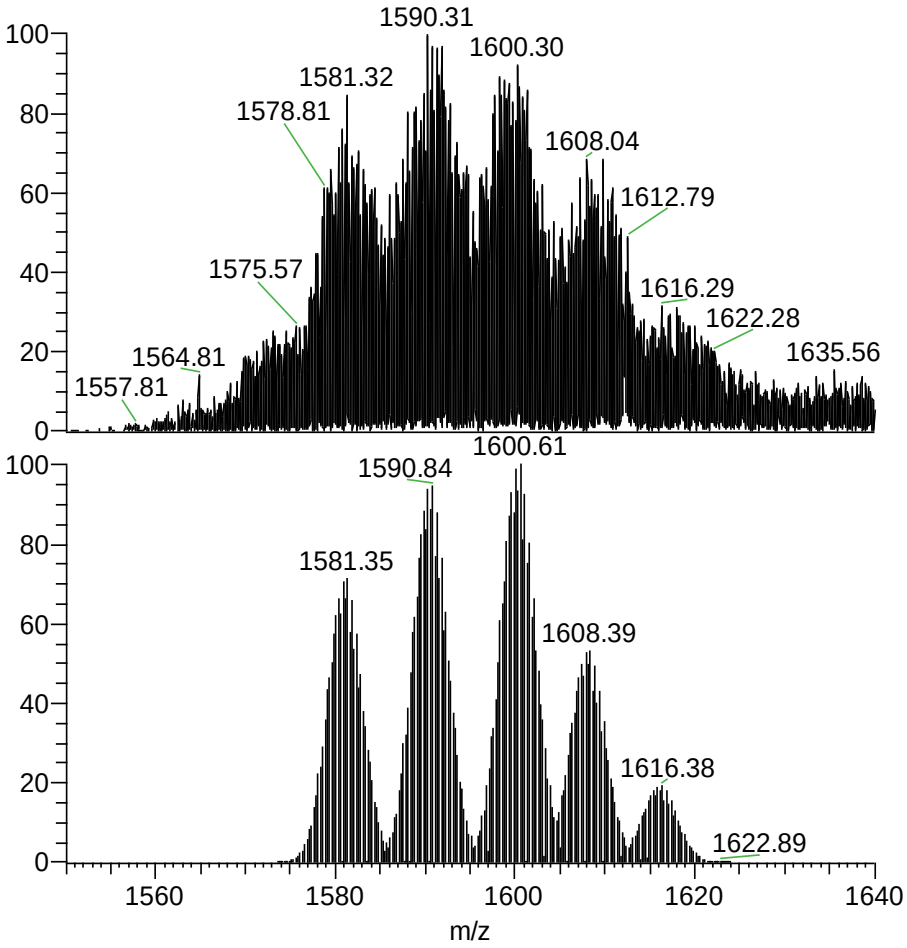

Figure S18. Comparison of the isotope splitting observed experimentally (upper part) and calculated for the –4 charged ion pairs based on the intact $[(C_6H_5PO)P_4W_{24}O_{92}]^{18-}$ polyanions (bottom). For the peak assignments see Table S8.

Table S8. Assignment of the signals from mass spectrometry (given as the value of the most abundant isotopologue) according to the simulation presented on Fig. S18.

Ion pair	m / z (calc)	Relative contribution to the simulated spectrum
$\{(DMA)_2K_2Li_2H_8[(C_6H_5PO)P_4W_{24}O_{92}]\}^{4-}$	1581.35	0.70
$\{(DMA)_2K_3Li_2H_7[(C_6H_5PO)P_4W_{24}O_{92}]\}^{4-}$	1590.84	1.00
$\{(DMA)_3K_3LiH_7[(C_6H_5PO)P_4W_{24}O_{92}]\}^{4-}$	1600.61	1.00
$\{(DMA)_4K_2Li_5H_3[(C_6H_5PO)P_4W_{24}O_{92}]\}^{4-}$	1608.39	0.70
$\{(DMA)_4K_3Li_4H_3[(C_6H_5PO)P_4W_{24}O_{92}]\}^{4-}$	1616.38	0.25

IX. References

[1] R. Contant, *Inorganic Synthesis*; Ed: A. P. Ginsberg, John Wiley and Sons: New York, **1990**; *27*, 104–111.

[2] CrysAlisPro, Agilent Technologies, 1.171.36.28 (release 01-02-2013 CrysAlis171 .NET).

[3] G. M. Sheldrick, *Acta Cryst.* **2008**, *A64*, 112–122.

[4] I. D. Brown, D. Altermatt, *Acta Crystallographica Section B Structural Science* **1985**, *41*, 244-247; *K. Knížek, Kalvados – Software for crystal structure and powder diffraction; see http://www.fzu.cz/~knizek/kalvados/index.html*.

[5] (a) M. Barsukova, N. V. Izarova, R. N. Biboum, B. Keita, L. Nadjo, V. Ramachandran, N. S. Dalal, N. S. Antonova, J. J. Carbó, J. M. Poblet, U. Kortz, *Chem. Eur*. **2010**, *16*, 9076-9085; (b) L. W. Daasch, D. C. Smith, *Anal. Chem*. **1951**, *23*, 853-868; (c) K. A. Jensen, P. H. Nielsen, *Acta Chem. Scand*. **1963**, *17*, 1875-1885.